Korean J. Chem. Eng., 37(1), 19-36 (2020)
DOI: 10.1007/s11814-019-0404-x

pISSN: 0256-1115
eISSN: 1975-7220

Flow characteristics within the wall boundary layers of swirling steam flow in a pipe comprising horizontal and inclined sections

Afrasyab Khan*,†, Mohd Sobri Takriff*, Masli Irwan Rosli*, Nur Tantiyani Ali Othman*, Khairuddin Sanaullah, Andrew Ragai Henry Rigit**, Ajmal Shah***, and Atta Ullah******

*Faculty of Engineering & Built Environment, Department of Chemical & Process Engineering, National University of Malaysia (UKM), Bangi 43600, Selangor, Malaysia
**Faculty of Engineering, Department of Mechanical Engineering, University Malaysia Sarawak (UNIMAS), Kota Samarahan 94300, Sarawak, Malaysia
***Center of Mathematical Sciences (CMS), Pakistan Institute of Engineering & Applied Sciences (PIEAS), Nilor, Islamabad, Pakistan
****Department of Chemical Engineering, Pakistan Institute of Engineering & Applied Sciences (PIEAS), Nilor, Islamabad, Pakistan
(*Received 8 May 2018 • accepted 12 October 2019*)

Abstract−Handling and utilization of steam flow efficiently to obtain various tangible industrial outcomes relies mainly upon how to optimize various flow parameters like boundary layer thickness, skewness, shear stress, and turbulent dissipation for minimum losses such as pressure and heat. Swirling steam flow, driven by a propeller through a circular duct along horizontal and inclined surfaces presents an interesting flow regime that includes the boundary layer flows close to the wall of the pipe and weak and uniform flow that prevails across the inner region of the pipe. Such flow was investigated here with a specially designed experimental facility. Convective Instabilities were observed that propagate along the axial direction in a nonlinear fashion. It was observed that the operating conditions could be optimized for measuring the shear stresses based on the intersection of the profiles under the effect of variations in the inlet pressure of steam and the rotational speed of the propeller. We found that the flow transformed from positive to negative skewness when the rotational speed of the propeller was raised from 4-14 thousand per minute at 10 bars of constant inlet steam pressure. More area came under the effect of reduced skin friction when the rotational speed of the propeller was raised. More turbulent energy was found to be dissipated when the rotational speed of the propeller was raised. It was found that yet the dissipation of the turbulent energy takes place under the joint effect of inlet pressure of steam and the rotational speed of the propeller, but the exact effect of any one of these two operating parameters still needs to be determined and requires further investigation.

Keywords: Steam, Swirl, Instabilities, Intensity, Skewness, Boundary

INTRODUCTION

When a fluid flows through a pipe, it faces forces along radial, tangential and axial directions. However, when the fluid is forced to flow using propeller or fan, the typical flow, being observed can split itself into multiple regions based on the kind of fluid and the phase and characteristics of the flow chamber as well as the flow regime [1]. Such flows in pipes present a unique scenario consisting of a no-slip condition at the boundary walls, resulting in pressure gradients between the wall and the boundary of the central core region, disturbing the flows ranging on the other side till fluid locks as in case of multiphase flows [2]. Such flows may pose severe issues to the industries where either steam is flowing as single-phase inside the pipes (e.g., steam turbine's pipes and rectangular ducts) or when steam is used as means for transporting the high-density materials (e.g. hydrocarbons). In the former case, the steam exerts pressure on the joints, bends and the corners, which ultimately has resulted in steam initiating rupturing of pipes, whereas in the later conditions, steam as being the gaseous phase travels above the hydrocarbons, the lower layer since having the rich viscous polar property interact with top steam layer and results into locks [3]. In recent times, there has been an increase in the depleted oil reserves inside the crest of the earth, thus requiring efficient and economical horizontal/inclined oil well drilling and extraction practices. On the other hand, in the case of the offshore explorations, the crude oil has been mainly brought to the shore by sub-sea jumpers that stretches along vast distances at the sea beds mostly in horizontal and slightly inclined orientations. It is, therefore, the flow of the fluids involving steam or the flow of the steam alone (steam turbines) inside horizontal pipes with or without bends that presents a problem to the scientific community to cope up with the optimization requirements for these processes [4]. Tackling a single aspect of above-discussed phenomenon, i.e., steam flow lines under the effect of the axial curvature of the pipes, centrifugal effect of the high-speed flows induced by the propellers, and superpositioning of the swirls producing skewness in the flows at the boundary layers presents a

†To whom correspondence should be addressed.
E-mail: drafrasyabkhan7@gmail.com

complex flow regime which needs to be investigated.

When steam moves in a pipe, the shear layer near the wall is affected by the changes in the turbulence structure of the flow. These changes in the turbulence structures are imparted by the curvature of the steam's flow streamlines. It is important to emphasize that these changes have a more significant effect on the flow as compared to the mere differences of pressure drop across the flow pipelines, since these changes considerably affect the shear and bring variations in the flow regimes and their structures within the boundary layers across the pipe. Additionally, for high speed flows in a pipe, Taylor Görtler vortices along the pipe length dominate the flow [5-10]. For proper understanding of such flows, the behavior of fluid, flowing at high speed in the pipes with horizontal and inclined orientation and the physical characterization and description of the regions within the wall layers across the pipe in such flows, has attracted huge attention from the scientific community for many decades. However, in the present case, instead of working on fluids like air, the scenario has been investigated when steam is flowing in swirl configuration inside the horizontal and inclined oriented pipeline. The reasons of this are two-fold: first, there is seldom a work being cited in the swirl configured steam flow in a pipe, and second, the investigations highlighting physical phenomena in such configuration can open further opportunities for academic and industrial communities to work on myriad phenomena hitherto unexplained, especially in industries, where steam is the major flowing fluid for transportation or used alone in industrial processes. It is within context of the article to present here the relevant work performed so far on the topic in the preceding paragraph.

There have been many studies on the topic of boundary layer for circular and rectangular duct flows with or without inclination. These studies focus both theoretically as well as experimentally, e.g., on the creation of the vortices and their breakup along the surfaces as well as the effect of the concave and convex surfaces in terms of stabilization of the boundary layer in case of turbulent motion [11,12]. The role of a surface having curvature in the axial direction in disturbing the turbulent flow has been discussed [6,13] extensively. Differing a little from the previous studies as has been viewed in the cited literature [14,15], the boundary layers in case of supersonic flows have been studied. The boundary layers have been subjected to a combined effect of pressure gradients, bulk dilation, and inclination. The Görtler vortices have been formed and propagated along axial direction in a flow channel; however, their effect on the boundary layers could not be found due to the limitations in the experimental facilities [16]. Still, the results have shown consistency in terms of stretching of the wake in the supersonic flow conditions [17]. The rest of the important quantities like the heat transfer [18] and skin friction [17,19,20] show significant increase as far as transformation from subsonic to supersonic takes place. Such claims have been proven further by the variation in pressure alone [21-23]. On the theoretical front, most recently the stability of the explicit methods in 2D cases and the extent to accelerate the computation of the coupled model of LBM have been investigated along with the investigations on the implicit solution of the RANS model in 3D [24]. Studies like these and others [25-29] in line with similar research objectives are useful for transient simulation of mixing processes & aerodynamic studies on different spatial and temporal scales.

From the studies given above, there is no literary citation, best known to the authors of the present manuscript, being seen in which steam flowing in swirling configuration, flowing over a surface with inclination has been discussed, to characterize for in-depth analysis of the fluid region near the boundary walls. This aspect of high-speed swirly steam flowing in swirl orientation over a horizontal and inclined surface of a pipe along with longitudinal curvature flow path needs attention and the current research manuscript is an effort in this regard.

Here, an attempt was made to highlight the different regions of the steam flow that have been accelerated first by the inlet pressure and subsequently by the propeller in a horizontal pipe with an inclined section at the later part of the pipe. Extensive experimentations were performed within a horizontal and inclined section of the pipe. Pressure sensors connected to the data acquisition system (DAQ) were used to determine the static and total stagnation pressures, which were then used to calculate the values of bulk, radial, axial and tangential velocities, head loss, skin friction, tangential shear stress, and turbulent dissipation energy, etc. The experimental setup is explained in detail in the proceeding section along with the outcomes and results in the subsequent sections.

EXPERIMENTAL SETUP

The experimental setup is comprised of a flow channel having an inner diameter, 0.153 m, and length, 15 m, whereas 10 m of the length is a horizontal section and the remaining 5 m of the pipe is inclined at 30 degrees from the horizontal axis. The thickness of the pipe wall is 25.4 mm (1 inch) and there are arrays of holes made at the lower surface of the channel along the complete length of the pipe as shown in Fig. 1. The outer surface of the pipe is wrapped with heat insulating material (Teflon) to secure the inner of the pipe from the surrounding temperature except for the holes where pressure sensors have been inserted using lip seals. The inner surface of the pipe is PVC pipe; thus the stainless steel pipe of which the flow channel has been made is sandwiched between these two heat-insulating materials. To preserve the uniformity of the steam content inside the flow channel, two types of the precautions were taken with one as previously discussed, the flow channel was insulated from the inside as well as outside with the PVC pipe and Teflon wrapping. In addition, the pipeline at the inlet of the flow channel pipe has temperature sensors (LM35) [30] all around its wall that give information about the temperature of the steam content exactly at the inlet of the pipe before the propeller. The quality of the steam was kept constant before the inlet to the pipe little above than the desired pressure (Pinlet ~11 bar) to ensure that the pressure drop in the main flow channel plus the temperature conditions would not affect the quality and content of the steam used for this study. There are around 100 holes being made along the complete length of the pipe and they have been located at equal distance from their corresponding geometric centers. 74 holes were drilled through the pipe along the horizontal section and 26 holes along the inclined section, as shown in Fig. 1(a). These holes serve both static and traversing total pressure measurements. Those holes, which were not in use during experimentation, are closed with screw bolts. Fur-

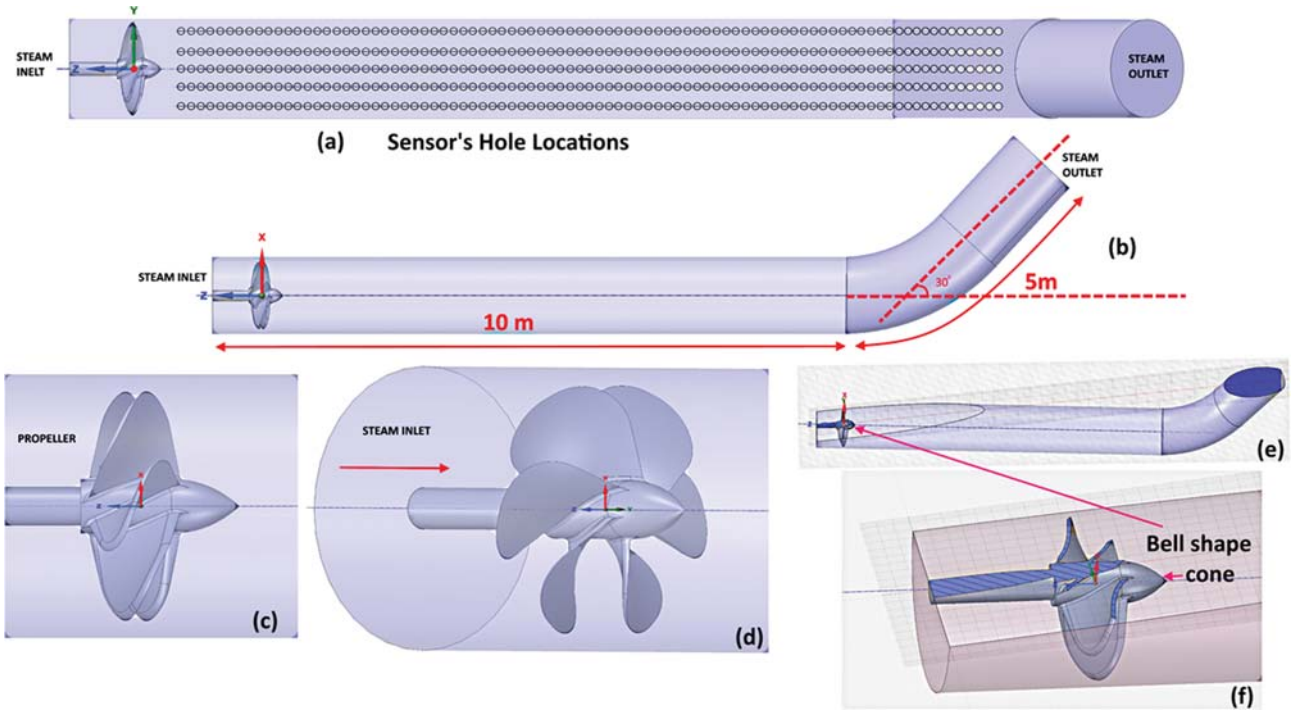

Fig. 1. Experimental setup, (a) Sensor's hole locations, (b) dimensions of the setup, (c) propeller, (d) propeller in an orientation showing no of fins, (e) cross-sectional view showing distance between propeller wings and inner walls and (f) propeller's view to show bell shape cone at the front of swirler.

ther, the presser sensor arrays are connected to a bar which can move vertically up or down to move the pitot tube pressure sensors in a radial direction (Fig. 2). This facility helps the pitot tubes pressure sensors to traversed across the pipe from position r=r, till the position r=0 to measure values of the stagnation pressure.

Care was taken that the surface of the bolt exposed inside the flow channel should be flushed with the internal concave surface of the channel in both horizontal and inclined sections to avoid any obstruction to the flow due to their physical size. The static pressure sensors are connected to the flow pipe in such a way that only their diaphragms should be exposed to the flowing steam. An industrial boiler (35 MW) was used to provide steam at a stable working pressure up to 25 bars and swirler/propeller was applied to generate steam's swirl flow in the pipe.

The pressure sensors [31] were inserted into the static holes by use of special purpose fittings that only expose the diaphragm of the sensors being flushed to the pipe's inner surface. The alignment of the pitot tube pressure sensor and the static pressure sensor was made in a way as shown at the top of Fig. 2 and Fig. 5(a). The lines passing through their geometric centers should cross at 90 degrees to each other. It was also taken care that the distance between the two pairs of sensors should be kept as much as the flow profile at the front or wake produced at the back of sensors should not affect the measurement of the adjacent sensor. Any misalignment may promote the occurrence of more elongated wakes in the flow channel, thus disturbing the measurements by the pair of downstream sensors, which can be avoided by following the above-stated provision strictly. The motivation for this study emerged from the fact that as the subsea pipes & jumpers are used to convey the crude oil from the deep crests below the bottom of the sea surface, therefore, steam has been used to facilitate the transport of the crude oil and other compounds inside these jumpers. These jumpers are lying on the bed of the sea and are stretched to the on-shore refining facilities in horizontal and inclined orientations. To ensure the flow assurance for the maximum flow, the flow inside these jumpers, which is comprised of a combination of gases, steam, crude/condensate, and water together with organic and inorganic solids (hydrate, scale, wax/paraffin, sand, and asphaltenes [32] etc.), that presents a complex flow phenomenon. These constituents of the flow inside these pipes/jumpers are a major reason for the blockage of these pipes, jumpers and other equipment in the subsea operations. Thus, the study of the flow of steam in the swirling configuration near the boundary walls was done that resembles the subsea inner flow profiles of these pipes. The pipe used in the current study resembles not only in terms of the flow orientation (swirling), but resembles in terms of horizontal and inclined sections with the subsea pipes as well.

1. Experimental Methods

Three rounds of experiments were performed. In the first, a reference inlet pressure and rotational speed of the propeller were set to a minimum level (P_{inlet}=4-5 bars and RPM=1,500-2,000); this was performed just to check that the flow can sustain itself and some reasonable values for the static and stagnation pressure were obtained by the respective sensors mounted at the start till the end of the horizontal section. In the second round of experiments, inlet pressure of the steam was raised from 10 bar of gauge pressure till 20 bars at an increment of 1 bar in each step, while keeping the propeller rotation speed constant at 4,000 rpm, whereas in the third round, the inlet pressure of steam was kept at 10 bars but the pro-

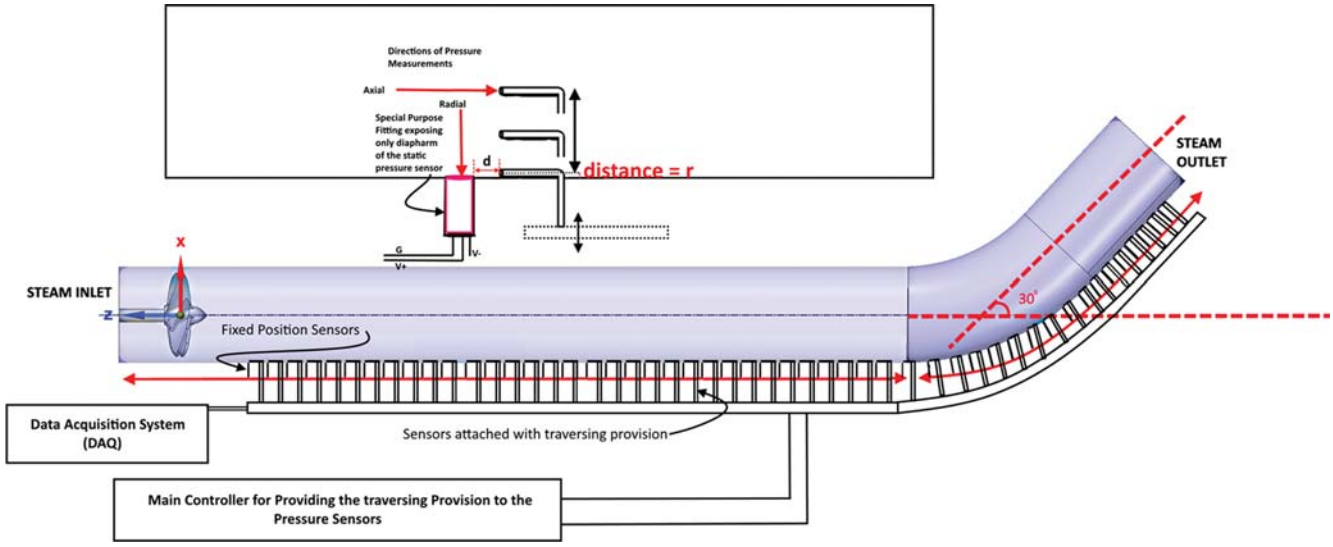

Fig. 2. Sensors with fixed and traversing provision inside the flow duct.

peller speed was raised from 4,000 till 14,000 rpm at an increment of 1,000 rpm in each step. All the pressure sensors were calibrated to the flows with steam prior to performing the experiments. Also, keeping in view the fluctuating nature of the data, all profiles were plotted with the best linear fit line to the least values of the data. The purpose of this caution is to ensure the said phenomenon exists even with the least values recorded in each experimental round. Measurements were recorded twice with each experimental run to check the spatial and temporal stability of the data.

2. Static and Stagnant Pressure Measurements

Both static and stagnation pressure measurements were conducted by following the scheme as illustrated in Fig. 2. The pressure at the main core region was measured with pitot tube pressure sensors by traversing them from position r=r till position r=0. Since the pitot tube cannot be very near to the wall of the channel due to the curved shape of the duct housing pitot pressure sensor in its middle section. For evidence of certain phenomena, such as convective instabilities at the wall of the flow channel, the readings of the pitot tube pressure sensors and static pressure sensors mounted at the walls of the flow channel were used.

The normalized longitudinal velocities in the most approximate locations of the wall were estimated with the core velocity behind the propeller, which is termed as mean bulk velocity U_m, static pressure P_{static} at the wall measured by the static pressure sensors and the stagnation pressure $P_{stagnation}$ measured by the pitot tube pressure sensors as shown in Eq. (1) [33],

$$\frac{V_{average}^2}{U_m^2} = 2\left(\frac{P_{stagnation} - P_{static}}{\rho U_m^2}\right) \tag{1}$$

where, U_m is an average axial core velocity behind the propeller/swirler (vol. flow rate/area), $V_{average}$ is the average velocity calculated here and g is the acceleration due to gravity.

3. Frictional Pressure Drop Measurements

Resistance imparted by the pipe's surface to the flow causes pressure loss, which is appropriately referred to as frictional pressure loss and can be characterized by the shape of the boundary layers [34]. Friction factor, characteristic of frictional pressure drop, was calculated numerically [35-37] using Colebrook-White equation for turbulent flows [38],

$$\frac{1}{\sqrt{f}} = 1.14 - 2\log\left[\frac{e}{D} + \frac{9.35}{Re\sqrt{f}}\right] \quad \text{for} \quad Re > 4000 \tag{2}$$

where f is the friction factor, D is the pipe diameter, e is the pipe roughness (for simplicity zero value has been considered as for a smooth surface (PVC with e~0.0015 mm) in the present case) and Re is the Reynolds number, which is expressed as,

$$Re = \frac{D\rho V}{\mu} \tag{3}$$

where ρ is the steam's density, V is the velocity based on the steam's mean flowrate and μ is the steam's dynamic viscosity. The friction factor "f" has been used in Darcy Weisbach relation [39] to calculate the head loss, h_f,

$$h_f = f\left(\frac{L}{D}\right)\left(\frac{U_m^2}{2g}\right) \tag{4}$$

where L is the length of pipe across which the frictional pressure loss has been measured. It was found that pressure head loss is maximum in the region near the propeller, whereas it keeps on decreasing along the length of the flow channel from a position l_0=10 cm till l=10 m (end of the horizontal pipe section as shown in Fig. 3). Yet in the present case, at any instance of time, the pipe cannot be considered empty from the air which may flow inside the pipe prior to the time when the steam flow in swirling configuration starts and the flow profiles become matured. But for the sake of simplicity we used Colebrook-White equation here for turbulent swirling steam flows by considering that either there is no air inside the flow pipe, or if still there is some air present inside the flow pipe, then it may exist at the same temperature as the steam, plus it will not affect the flow profile of the steam as it exists at atmospheric pressure inside the said flow pipe prior to the time when measurements were done. These suppositions were made

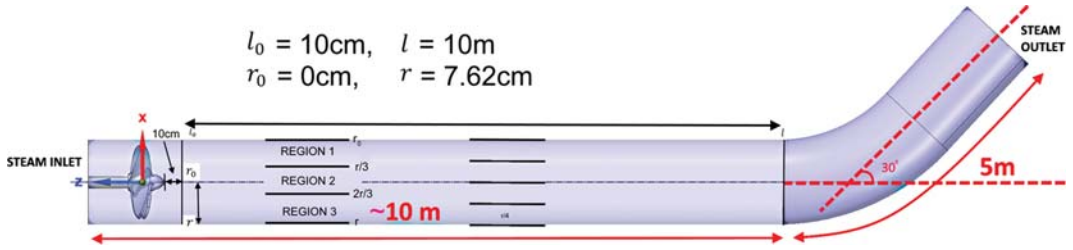

Fig. 3. Dimensions along which measurements have been taken inside the pipe.

only for the calculations of the pressure head loss in the straight channel, and not for the inclined channel.

RESULTS AND DISCUSSION

The results obtained and subsequent discussion on them are presented under two sections, the first section comprises the flow characterization along the horizontal section and the second section is related to the flow characterization along the inclined section of the pipe.

1. Flow Characterization Along the Horizontal Section

The Flow in the horizontal section has been characterized based on the properties of the swirly flowing steam as follows.

1-1. Convective Instabilities Within Wall Layer of the Channel

It is well known that the turbulent structure of the flow depends on the operating parameters. The disturbances across the boundary layer affect the turbulent shear layers, and the thickness of the turbulent shear layer depends on the nature of the instabilities (e.g., convective, KH instabilities, etc.) [14]. Further, the radial curvature of a channel affects the properties of the flow. This affects the core region flow in the form of the uneven pressure gradients or narrowing the diameter of the flow channel in the case of the viscous fluids (e.g., non-slip condition), thus becoming a source of degradation, if viewing this problem from the point of view of

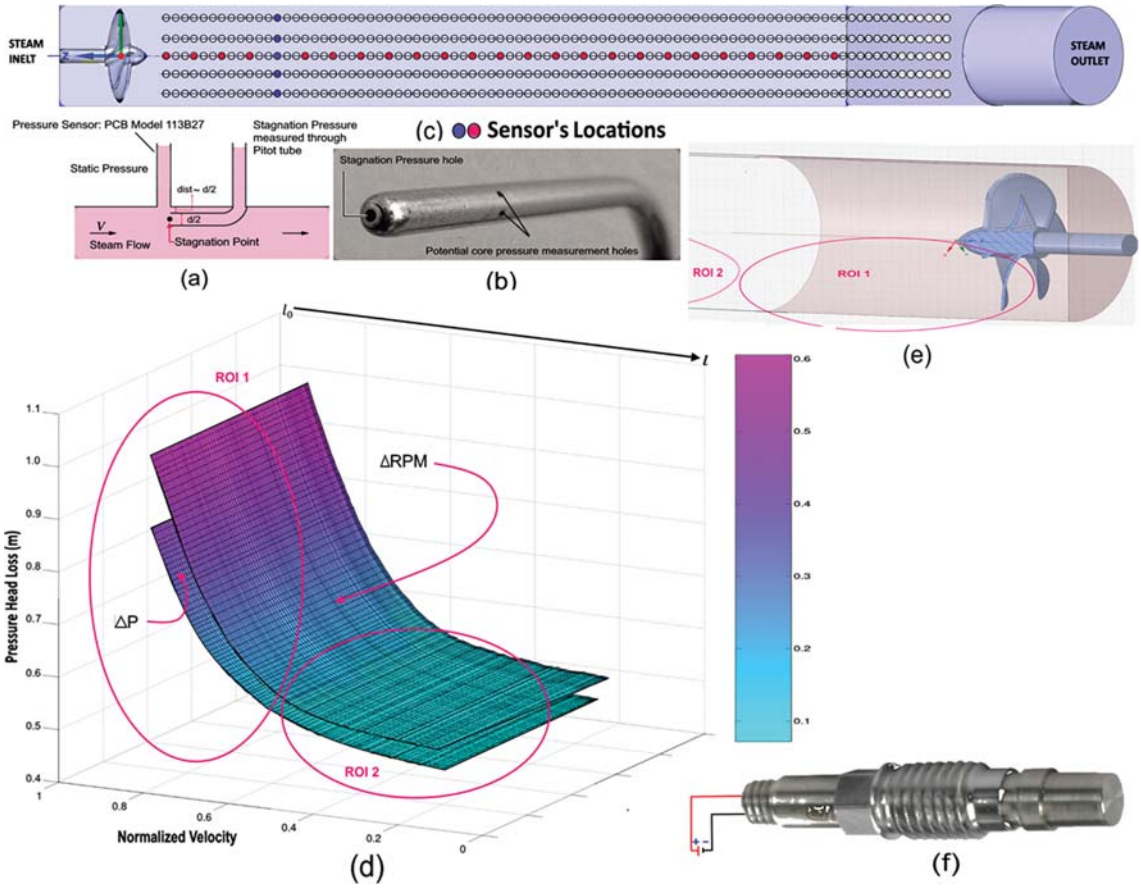

Fig. 4. Pressure head loss profile under varying inlet steam pressure and swirler rpm. (a) Orientation of sensors for measurement, (b) pitot tube pressure sensor, (c) location of sensors in axial and radial direction at the bottom of the pipe, (d) 3D profile for pressure head loss along axial direction and (e) ROI 1 & 2 (f) static pressure sensor.

proper pressure distribution inside the flow channel as discussed in the cited literature [14]. In case of flow channels, longitudinal vortices may develop near the wall, which dominates the core region flow and beyond it till the boundary layers as cited before [14]. Here, in the current manuscript, the occurrence of the penetrative convective instabilities in the near-wall regions was disclosed. These instabilities were generated under the action of buoyant convective forces alongside and normal to the boundary walls. Further downstream, along the wall, these instabilities take the form of the vortices producing a nearly wavy like flow profile at the wall of the channel [14].

In the present case, due to the convective flow and centrifugal force being exerted by the propeller, significant axial pressure gradients were developed, which was evident from the static pressure (P_{static}) and stagnation pressure ($P_{stagnation}$) measurements, and velocity calculations as presented in Fig. 4(d). Convective instabilities at the location along longitudinal direction were measured with the help of the spatially varying static and pitot pressure sensor's values. Normalized pressure values $\frac{(P-P_{static})}{(P-P_{stagnation})}$ were measured from the readings of both sensors. These measurements along with Eq. (1) and further equations related to pressure head loss (Eqs. (2)-(4)) as given in previous sections were used to find the pressure head loss versus the variation in velocities near the boundary wall region along the longitudinal direction of the pipe.

1-2. Wall Effects

From Fig. 4(d), it has been found that pressure head loss varied along the axial direction in a decreasing fashion. During the second and third round of experimentation, i.e., (ΔP and ΔRPM), the pressure head loss was maximum near the position corresponded to l_0, whereas after that, the pressure head loss kept on decreasing till position l. Profile for the variations in rotational speed has higher pressure head loss values at any spatial position as corresponding to the profile for the inlet steam pressure. The possible reason for this trend is that in the case of the higher rotational speed, more and more steam was expelled towards the boundary wall region. Now as due to the static nature of the boundary walls the pressure exerted by the steam volume will be dissipated there, plus the flow is negatively skewed in the case of the ΔRPM (as will be discussed in the proceeding sections); therefore, the pressure head loss is higher in the case of the variation in rotational speed of the propeller at 10 bars in the regions near the propeller (Region of Interest-1 (ROI 1)). Afterward from there the difference between the values of pressure head losses for both ΔP and ΔRPM keeps reducing till the position l, but still, there a gradient exists between their values (as observed from Region of Interest-2 (ROI 2)).

Note that the readings of the pitot pressure sensor were acquired at the most approximate position near the boundary walls. It was observed that by varying the pressure and keeping the rpm of swirler at 4,000 rpm, a wavy like profile was observed as evident from normalized pressure across the axial direction. This behavior sustains approximately till the half of the pipe length, after that the profile becomes smoother, which warrants the decay of instabilities that can be seen in terms of their strength on pressure scale. The instabilities seem to diffuse through the longitudinally stretched fluid layers towards far regions across the whole length of the pipe's horizontal flow channel. Contrary to that, the variation in the RPM of the swirler imparts a more dominant effect as the fluctuations are very visible, higher in amplitudes, but only can be sustained till ~6.5 m of the total length of the flow channel. Afterward, the profile becomes smoother, which is evident from a large decrease in normalized pressure inside the near-wall region corresponding to ~r/4→r radially, along an axial direction. Such variations in the form of a dimensionless ratio for pressure loss can be regarded as convective instabilities which are penetrative in nature, which has been observed for the case of the swirling steam flow in the horizontal flow channel.

The flow downstream locations at which the pressure sensors record higher values of these fluctuations, i.e., crests, may correspond to when these flow instabilities are directed towards the wall of the flow channel, whereas the points at which the fluctuations are showing lower values, i.e., troughs, may be regarded as when the vortices creating the flow instabilities are directed away from the wall of the channel. The axial wavelength of these vortices in the near-wall region boundary layers was found in the range of ~3-3.7 m when the pressure was varied from 10 to 20 bars. Boundary layer thickness δ varied ~9% (ΔP)→~14% (ΔRPM), displacement thickness δ^*~3.8% (ΔP)→~5% (ΔRPM), whereas momentum thickness, θ varied ~0.8% (ΔP)→~1.2% (ΔRPM). These quantities were determined from Eqs. (5) and (6) as well as pressure-based measurements from two pair of sensors along the whole of the length of horizontal section; the equations for δ and θ are expressed as,

$$\delta^* = \int_0^r \left(1 - \frac{V(r)}{V_{near\ wall}(r)}\right) dy \tag{5}$$

$$\theta = \int_0^r \frac{V(r)}{V_{near\ wall}(r)} \left[1 - \frac{V(r)}{V_{near\ wall}(r)}\right] dy \tag{6}$$

Whereas $V_{near\ wall}(r)=V_{average}$ at r=~r, which has been measured using the same way as used for the measurement of $V_{average}$ using Eq. (1). An important aspect was found in the spatial and temporal non-frozen nature of these vortices. As the repeated experiments revealed that the vortices change their position, which could be attributed to the asymmetric mode of propagation of the steam flow lines in a longitudinal direction.

The swirling flow of the steam, having an expanding tendency while being exposed to the ambient environment, the effects of the buoyancy and centrifugal forces acting on it, caused a complex flow structure. The streamlines of the steam flow were affected by the radial curvature of the walls of the channel (the inner concave surface of the pipe) in addition to the skewness added to the flow, when a considerable pressure gradient and variations in rpm of the propeller acted upon these lines along the radial and axial direction. Thus, a deep understanding of the effects due to the operating parameters on the flow structures, mainly through the regions near the boundary walls is vital. To address these issues, further investigations were performed to find the effect of the swirl intensity on the fluid regions near the boundary walls regions; the decay of the swirl intensity along with the role of shear stress towards profile shaping of these layers, was reported and discussed in the preceding sections.

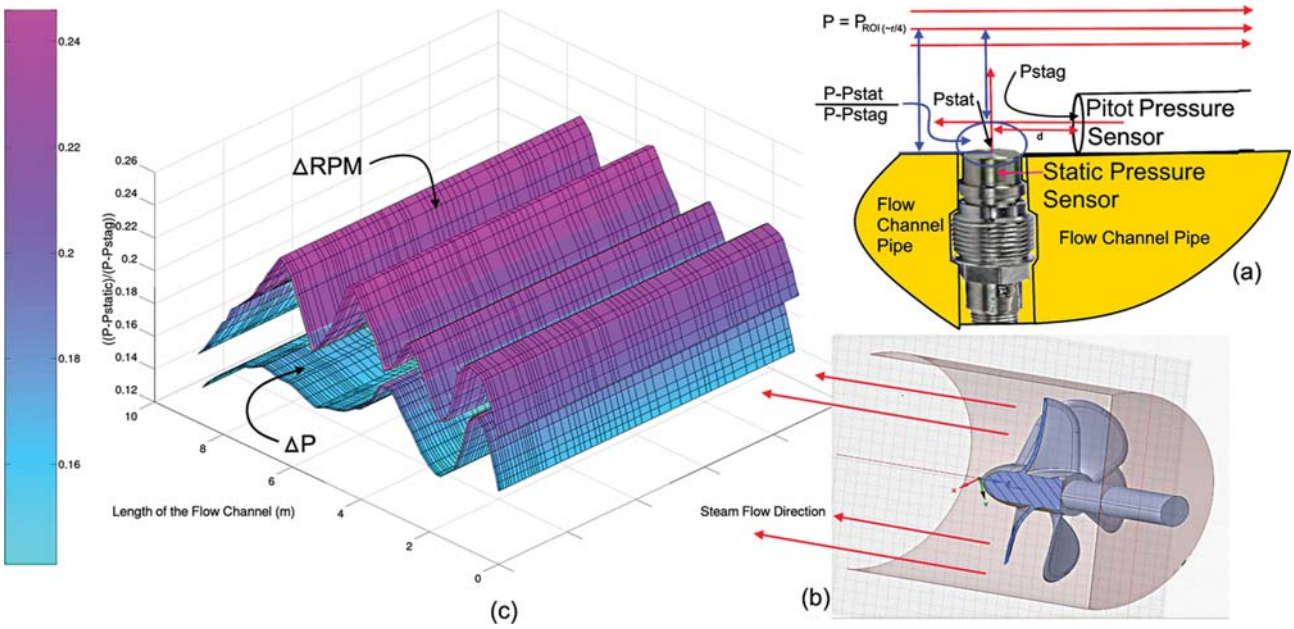

Fig. 5. Convective instabilities in the boundary layers, (a) orientation of sensors for measurement of pressure, (b) direction of flow of the fluids, (c) convective instabilities in terms of pressure fluctuations/variations along longitudinal direction in boundary layers.

1-3. Decay of Swirl Intensity Acting on the Boundary Layers

The steam's fluid domain moves in axial direction under the gradient of the pressure, upon which the centrifugally swirling oriented velocity components superimpose, which gives rise to vortices like structures [40] in the ROI and more prominently (as in present setup) inside the fluid layers near the boundary walls corresponding to r=r/4→r=r. These vortices have a decaying tendency in the far spatial positions along a longitudinal direction, whereas the flow structures, prevailing inside these flow layers, are subjected to the centrifugal force and shear stresses. To calculate the shear stresses acting on the fluid layers near the walls of the flow channel, where complex turbulent structures prevail in the near boundary wall layers, while steam flowing as swirly through the flow channel, is a challenging issue, which has been addressed here. The mean velocity components along the axial direction were measured with pitot tube pressure sensors, and in the tangential direction it has been calculated indirectly using the relation given below. Swirl intensity Ω was calculated along axial and radial directions using the relation [41,42],

$$\Omega = 2\pi\rho\int_{x_0}^{x} \frac{UWr^2}{\rho\pi r_0^3 U_m^2} dx \quad (7)$$

where, x=r, $l \rightarrow 7.62$ cm, 10 m & $x_0=r_0$ & $l_0 \rightarrow 0$, 10 cm. The tangential velocity was measured indirectly from the values of the rotational speed V_r of the propeller (4,000-14,000 rpm) and radius r of the flow channel (0.765 m).

$$W = V_r \times r \quad (8)$$

where U, is the mean axial velocity (measured with pitot tube pressure sensor at r=0), W is the tangential and U_m is bulk velocity (measured at the back of the propeller), l and l_0 are the axial positions corresponding to the point at a distance of 10 cm (on the boundary wall corresponded to l_0=0) from the tip of the bell shape cone at the front of the propeller at which measurement was taken (Fig. 5) and length l=10 m of the flow channel, respectively.

Pitot tube pressure sensors were traversed through the hole which is at position l_0 axially, from a position r_0 till r as shown in Fig. 5. By considering the effect of the pressure and rpm on the velocity of the swirling steam flow, the profiles for the normalized swirl intensity decaying along the axial and radial directions were plotted in Fig. 6.

From Fig. 6, along the axial direction, the swirl intensity has the maximum value which gradually decreases as the steam moves downstream along the axial direction. An exponential drop for swirl intensity can be seen in the region corresponding to the downstream distance 4.5 to 5.5 m when the steam inlet pressure varies from 10-20 bars at 4,000 rpm of the swirler. Whereas, there is a gradual decrease in the values of the axial and tangential velocities measured at these locations, as compared to the bulk velocity U_m (measured at an approximate position l_0 to the propeller where the velocity is maximum). So, on the axial scale, 4.5-5.5 m corresponds to the length till which the swirl intensity keeps its strength before an exponential decrease in its value occurs, and this continues till the end of the horizontal section. The further exponential decrease in swirl intensity due to change in RPM occurs as compared to the decrease in the value of the swirl intensity because of change in inlet steam pressure. The possible reason for this may be that as with increase in pressure the flow has shifted more towards the axial central axis. The slope of the profile associated with ΔP is less than the slope of the profile related to the ΔRPM along axial direction. As the values for swirl intensification were calculated at the boundary wall regions, therefore, the variation in RPM shows an elongated profile on spatial basis till which the swirl intensity has sustained its values in a reasonable range. This elongated behavior

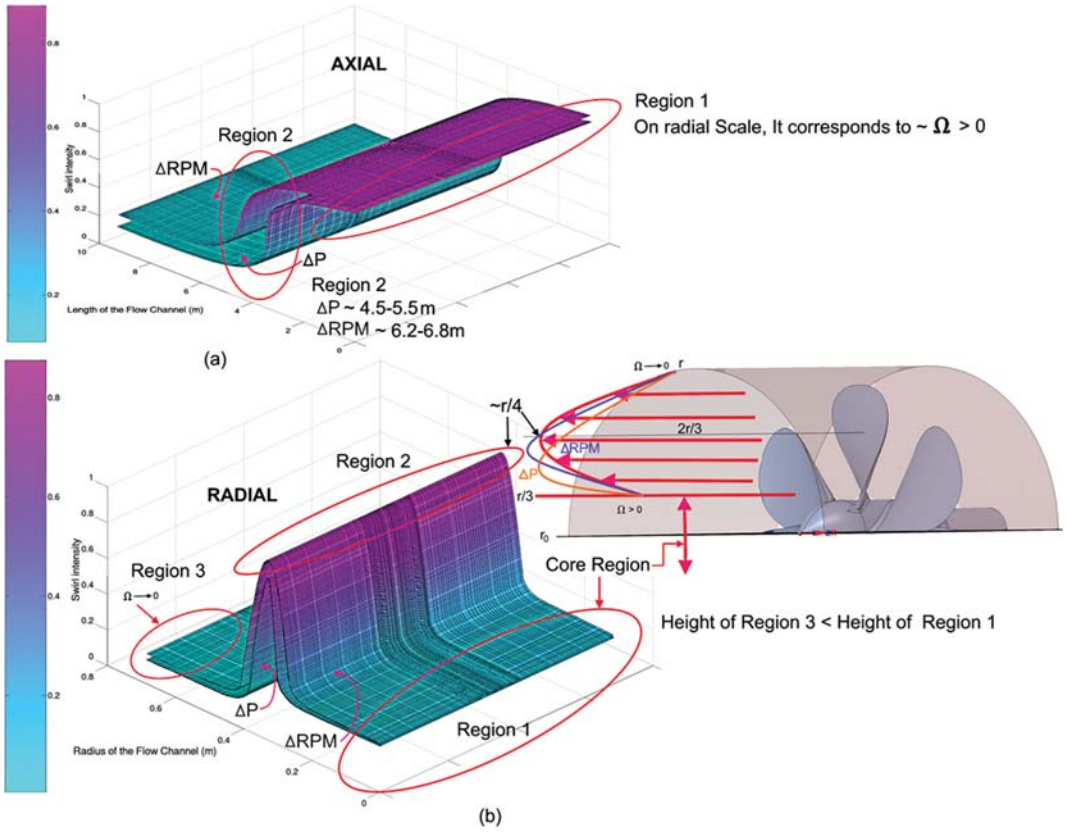

Fig. 6. Normalized swirl intensity profile, (a) along axial direction and (b) along radial direction.

can be attributed to the negative skewness of the flow profile while variation in rpm has been made at constant inlet steam pressure of 10 bars.

Along the radial direction, the whole region can be divided into three sub-regions. Region 1 corresponds to the region near the central core region corresponding to $r_0 \rightarrow r/3$, region 2 corresponds to the location where maximum velocity has been observed corresponding to $\frac{r}{3} \rightarrow \frac{2r}{3}$, as shown by Fig. 3, and region 3 corresponds to the region near the boundary wall, corresponding to $\frac{2r}{3} \rightarrow r$. It has been observed that the swirl intensity has maximum values in the area corresponding to $\frac{r}{3} \rightarrow \frac{2r}{3}$ radially, from the wall.

Note that the region corresponding to $\frac{r}{3} \rightarrow \frac{2r}{3}$ where the flow has shifted from positive to negatively skewed profile under the variation of pressure and rpm.

However, as approaching close to the boundary layers, the swirl intensity decreases and due to the physical size of the pitot tube, the value of swirl intensity (approaching to zero, $\Omega \rightarrow 0$) can only be determined till the point near the wall, where the tip of the stagnation pressure sensors can measure the pressure. Also, the swirl intensity decreases more rapidly when approaching the wall as compared when getting near to the core region; the possible reason for this behavior may be that the core region is not totally devoid of any fluid pressure, rather fluid's lower pressure prevails within the core region.

1-4. Decay of the Shear Stress Acting on the Boundary Layers

As the swirl intensity mainly decays due to the tangential wall friction, so to calculate the tangential shear stress $\tau_{r\phi}$ it has been derived from Eq. (7) by transforming it into cylindrical coordinates and the resulting Eq. (9) can be expressed as,

$$\tau_{r\phi} = \rho VW + \frac{\rho}{r^2}\int_0^r r^2 \frac{\partial}{\partial x}\left(UW + \overline{uw} - v\frac{\partial W}{\partial x}\right)dr \tag{9}$$

where $\tau_{r\phi}$ is the tangential shear stress, V is the mean radial velocity of the flow domain which was estimated from Eq. (1) by making use of pressure difference between the measured stagnation and static pressures, and u and w represent the average fluctuating axial, and tangential velocities, respectively. The normalized tangential shear stress is obtained by dividing $\tau_{r\phi}$ by the dynamic pressure of the moving fluid element, $\frac{1}{2}\rho U_m^2$ [43]. The normalized tangential shear stress [41,42] can be expressed as,

$$\frac{\tau_{r\phi}}{\frac{1}{2}\rho U_m^2} = 2\frac{d}{d\left(\frac{x}{2r_0}\right)}\int_0^{r_0} \frac{UWr^2 dr}{r_0^3 U_m^2} = \frac{1}{2}\frac{d\Omega}{d\left(\frac{x}{2r_0}\right)} \tag{10}$$

Similarly, the shear stress was normalized using the dynamic pressure quantity, which was measured at different inlet conditions involving a variation of the inlet steam pressure and rpm of the

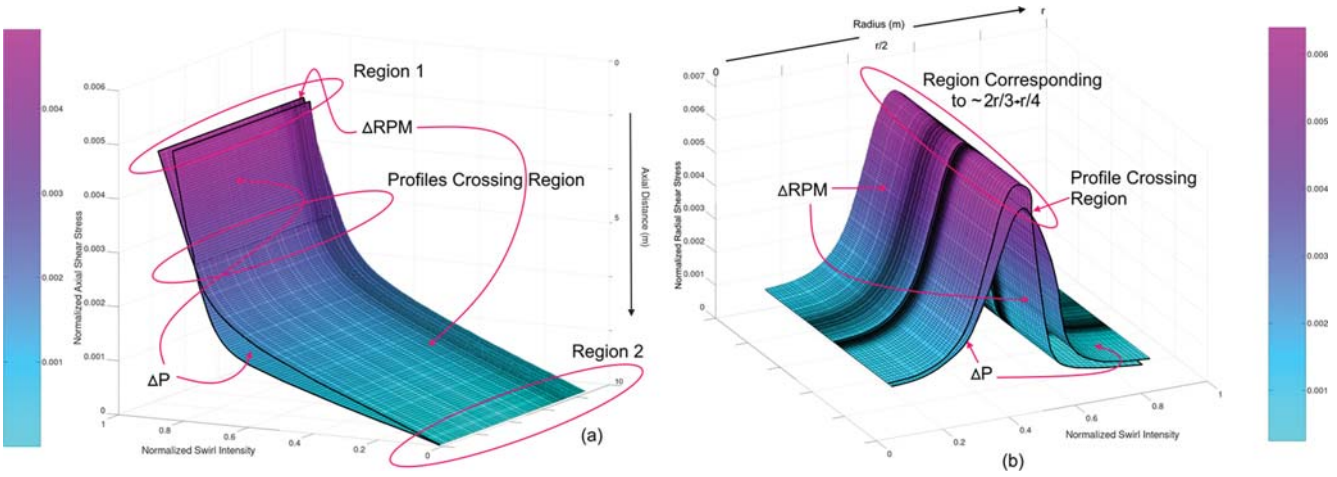

Fig. 7. The profiles of normalized shear stress vs normalized swirl intensity (a) axial (b) radial.

swirler. The profiles were plotted to keep in view the least values of the inlet conditions, i.e., keeping the inlet pressure fixed at 10 bars and varying the rotational speed of the swirler from 4,000-14,000 rpm @1,000 rpm per step; alternatively, keeping the rotational speed of the swirler fixed at 4,000 rpm and varying the inlet pressure from 10 to 20 bars @ 1 bar in each phase of experimentation. Profiles were plotted for the normalized tangential stress along the axial and radial directions to show the existence of the phenomena at the least available operating conditions. Profiles of normalized tangential stress versus normalized swirl intensity along axial and radial directions are shown in Fig. 7.

As seen in Fig. 7(a), the value of normalized shear stress increases axially with an increase in the normalized swirl intensity. At the region corresponding to 5-6 m along horizontal, the profile against the variation in pressure intersects with the profile of the normalized tangential shear stress for the variation in rpm, thus establishing a point for optimization that depicts that even the single input operating parameter (either ΔP or ΔRPM) can suffice for the purpose rather than varying the other till its higher values. The profile of normalized tangential shear stress, within the range 0.63-0.75 of normalized swirl intensity drops exponentially that has corresponded to 5.9-8.1 m (see Fig. 5) along the axial direction. Further, from ~4/5 L till the end of the horizontal section, i.e., l=10 m, the figure exhibits a smooth profile showing a decreasing trend till the end of the channel. This is due to the decrease in axial velocity, which was attributed to the increased thickness of the boundary layer that leads to non-uniform decrease in the values of the normalized shear stress versus the normalized swirl intensity along the downstream length. Thus, normalized swirl intensity and normalized tangential shear stress both have the same decreasing trend downstream of the flow channel along axial direction. Note also that the central core region is initially devoid of the high pressure due to the rotational speed of the propeller and the bell shape-like cone at the front of the propeller that expels the fluid more towards the annular region and beyond in the present configuration. However, when approaching the far end of the flow channel, the pressure of the central region $\left(0 \rightarrow \frac{r}{3}\right)$ has gained some value in comparison to the annular region $\left(\frac{r}{3} \rightarrow \frac{2r}{3}\right)$, because in the downstream region of the flow channel, it is due to the loss of the pressure inside the annular region and the region more specifically corresponding to r/4→r (near-wall boundary layers); thus due to this reason along the length scale beyond ~4/5 L till the end of the horizontal section, i.e., l=10 m, the decrease in the tangential shear stress is very gradual. Yet the profile for the ΔRPM has steeper slope as compared to the profile for the ΔP, which shows the effectiveness of the rotational speed of the propeller in imparting high shearing flow at large axial distances.

Along the radial direction, as shown in Fig. 7(b), the values of the velocities were measured with the pitot tube pressure sensor mounted at position l_0 (Fig. 5), whereas the pitot tube pressure sensor was traversed from position r_0→r. The profiles responding to ΔP and ΔRPM intersect each other in the region corresponding to ~2r/3→r/4 radially, whereas the peak lies somewhere between ~r/3−r/4. The normalized shear stress initially increases till its peak followed by decrease till the boundary walls. The profile has more height towards the central core region as compared to its height towards the boundary walls which shows that at the axial position l_0 when pressure sensor has been traversed from r_0→r, the central core region has certain amount of pressure and some contribution in terms of flow of the steam due to the rotational speed of the propeller.

Also, at the same swirl intensity, the value of the tangential normalized shear stress against normalized swirl intensity has higher value, which can be attributed to the rotation of the propeller to produce intense shearing flow in the present configuration as compared to the impact on to the shear due to the steam's inlet pressure. But this behavior was contradicted in the region corresponding to ~2r/3→r, as can be seen on the right-hand side of the flow profile in Fig. 7(b), which shows that in this region the pressure has become the dominant parameter, corresponding to l_0. This contradicting behavior was seen when the pressure measurements were taken by the pitot tube pressure sensor at successive positions, l_1=3 m, l_2=5 m, & l_3=7 m, so a possible reason for this behavior may be the narrowing of the flow channel with increase in pres-

sure and radial stretching of the flow with increase in rpm.

1-5. Skewness of the Flow within the Wall Layer

For turbulent flows at lower values of normalized swirl intensity, the flow skewness (i.e., when profiles for the velocity and temperature have been considered) reported in literature, was associated with a fixed value ~0.8 with any amount of variations in Reynolds Number [44-47]; this shows its independence on Reynolds Number. However, the negative skewness can never be explained if following the stated norm [48]. Now as the centrifugal velocity components due to the rotational speed of the propeller have been superimposed over the axial velocity components owing to the inlet pressure variations, so there will be vortices being generated and dominating the flow regimes that will be flowing in the regions near the boundary walls [40]. Thus, skewness of these flow regimes was investigated for the profiles of the normalized axial and tangential velocities. Distribution of the velocities in the region extend-

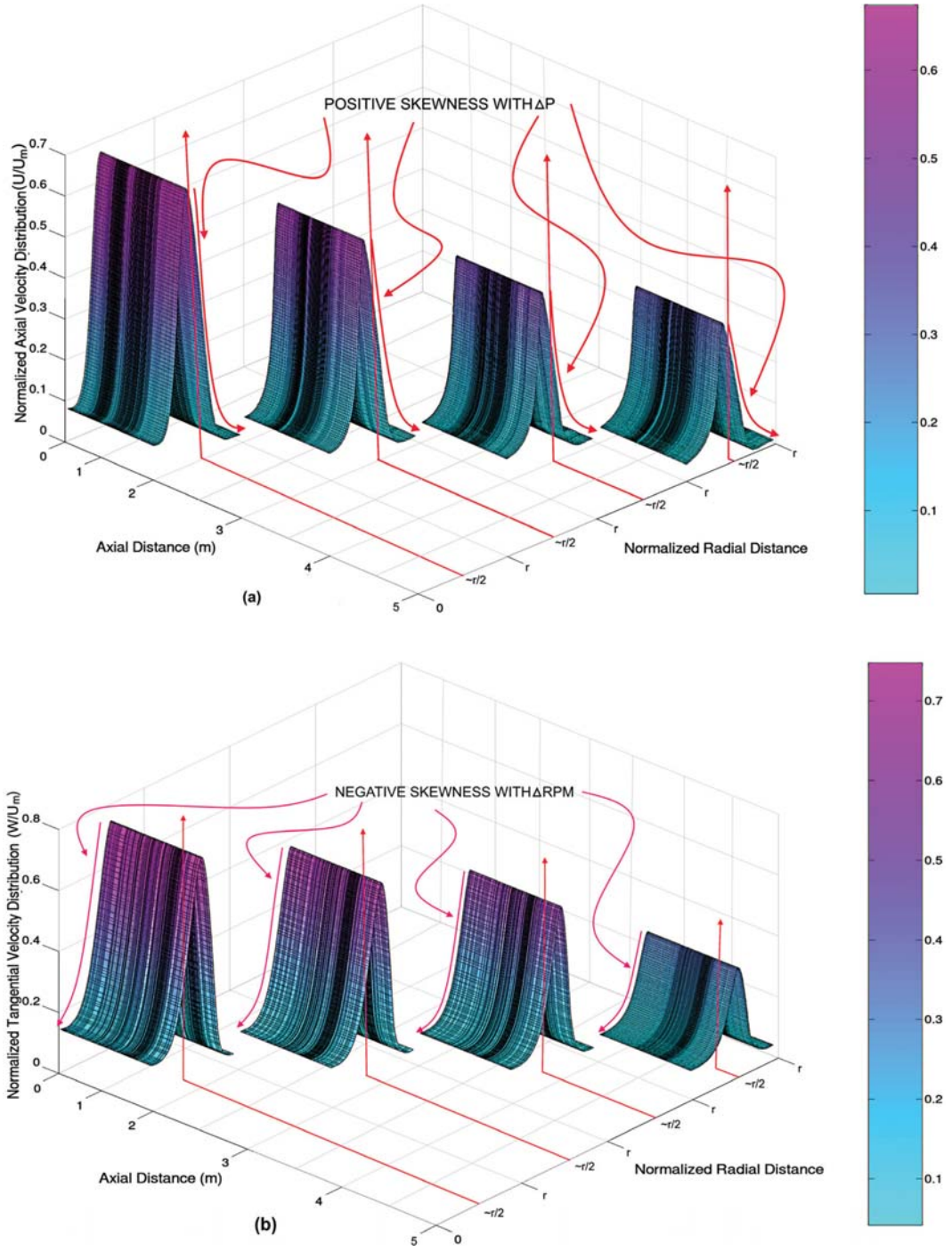

Fig. 8. Profiles for normalized velocities against variations in inlet steam pressure & rotational speed (a) axial (b) tangential (c) skewness comparison.

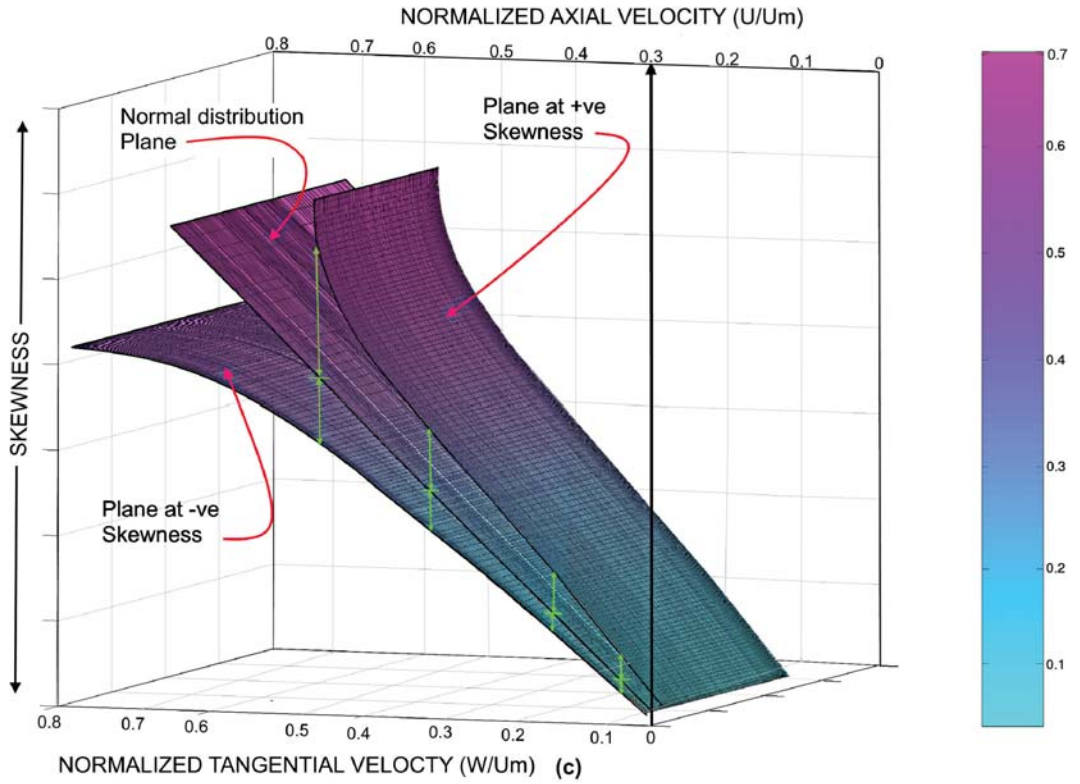

Fig. 8. Continued.

ing from r=0, till r=r, are shown in Fig. 8. Note that the axial and tangential velocities were estimated in the same fashion as described before at five different positions in the flow channel corresponding to $l_1 \rightarrow l_5 = 1 \rightarrow 5$ m.

A shift in the skewness was observed from positive to the negative when the data was acquired under two operating conditions: ΔP=10-20 bars and ΔRPM=4,000-14,000. The data was acquired using the pitot tube pressure sensor at positions from r=0, till r=r, and an axial distance ranging from $l_1 \rightarrow l_5$. Physically, this shift in skewness may be explained first by centrifugal force, as with rise in centrifugal force acting on the steam, which may quantitatively be associated with the rise in swirl intensity, more volume of steam will be expelled towards annular region and beyond it into the wall region. This enhanced movement of fluid streamlines towards the boundary wall region will contribute towards the shift of the skewness from positive to negative as shown in Fig. 8(a) and (b). Contrary to this, when the inlet pressure was increased, the distribution remained positively skewed, which forces it to move inside the annular region or more in an aligned fashion with the axial axis. It has been observed that the effect of increase in pressure on the skewness is not much dominant in the region ~r/4→r. This indicates that increase in pressure does not contribute too much in expelling of the fluid towards the boundary walls; rather more volume of fluid, i.e., steam was flowing in the annular region, which depicts a type of control mechanism for the fluid flow inside a channel with the present configuration. More flow-induced pressure can be generated inside the annular region as compared to the near boundary walls regions when fluid pressure has been raised from 10 till 20 bars. However, when the rpm was increased from 4,000-14,000, the fluid region shifted towards the boundary walls if the position ~r/2 is regarded as the normalized distribution in the present configuration. So, based on this analysis, it can be claimed that the increase in pressure does not contribute in terms of saturation of the turbulence near the boundary wall region, but increase in rotational speed of the propeller surely does. On comparative basis as shown in Fig. 8(c), it has been observed that more dominant effect was imparted by the axial velocity on the positive skewness as compared to the negative skewness as in case of variation in rotational speed. This comparative effect is shown by the vertical arrows inside the profiles which distinguish each profile (upward and downward side) from the normal distribution plane (traversed at the center). The axial velocity distribution, which was measured along the axial direction, has more steep profile as compared to the profile for the normalized tangential velocity distribution. Further, both the velocities were normalized using the bulk velocity U_m.

2. Inclined Section of the Pipe

The flow in the inclined section was characterized based on the properties of the swirly flowing steam as follows.

2-1. Steam Flow in an Inclined Channel

In characterizing the inclined section of the flow channel, variations, effects, and trends reported in the figures may not exactly be representing the same parameters which have already been discussed for the horizontal section of the flow channel. Rather, we attempt here to discuss those quantities which are more important in relation to the inclined section and carry physical and scien-

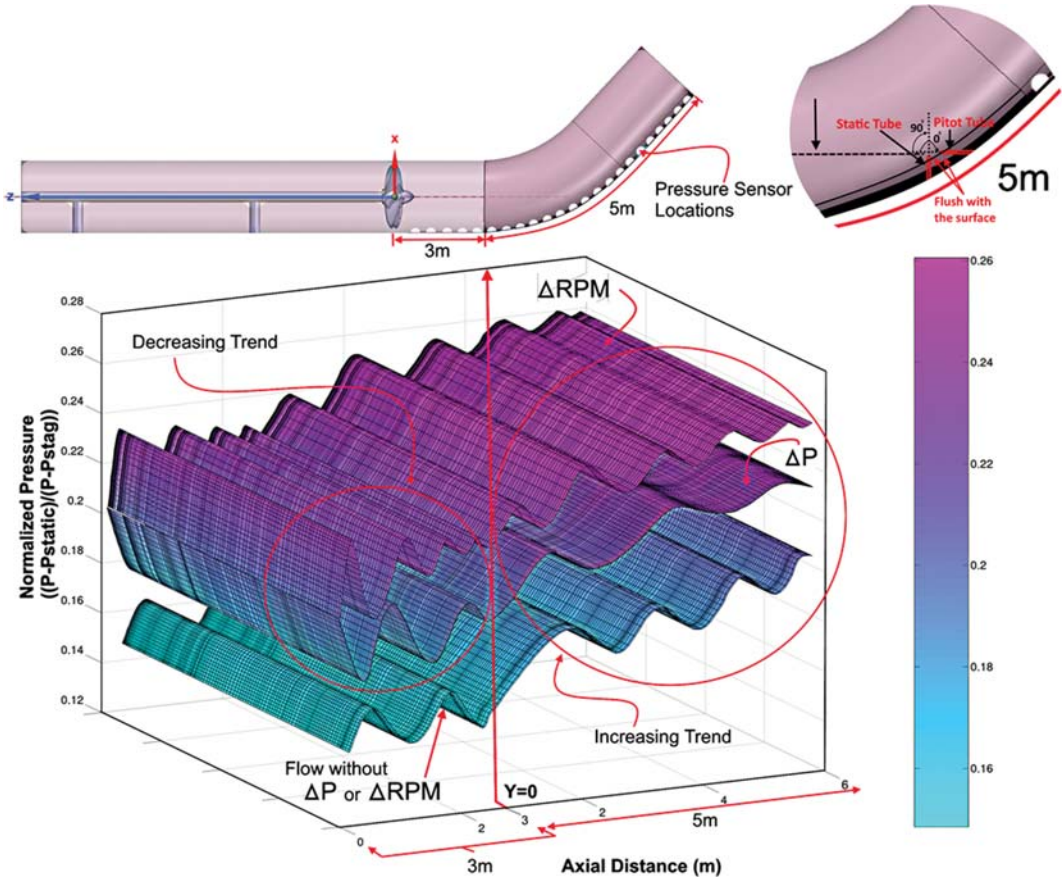

Fig. 9. Profiles for normalized pressure along inclined flow channel.

tific implications.

For consistency to the flow similarity between horizontal and inclined sections of the pipe, Reynolds number was calculated for the flow at the exit of the horizontal section after assuming non-existence of the inclined section. The Reynolds number was recalculated again after attaching the inclined section, and for sake of flow similarity, the propeller was brought forward in the horizontal channel as shown in Fig. 9 (see top section of the figure). After shifting of the propeller to ~7.3 m from its original position, towards the inclined section, the flow similarity based on Reynold's number was obtained in both horizontal and inclined sections of the pipe. When fluid enters the inclined pipe through the bend from the horizontal pipe, disturbances in the flow are created [49-51]; these disturbances affect the boundary layers as well as the flow regimes near the boundary wall layers. The pressure exerted by the flow is distributed over boundary layers due to the inclination of the flow channel [50,51]. Contrary to the pressure profiles in the horizontal section, where the pressure has dropped along the axial direction in the boundary wall regions, here along the inclined pipe, the pressure increases gradually. In the present case, the steam flow within the boundary wall region is influenced due to the pressure gradient, inclination, and expansion at the same time. In these types of flows, an additional shear acts upon the fluid within the boundary wall-flow region [14]. For flow through a surface having a longitudinal flow path with curvature, the effect of the pressure on the turbulence length scale and Taylor-Görtler vortices is well understood [14]; however, in the proceeding section, our main purpose is to investigate the variations in the flow structures in the near boundary wall region.

2-2. Interaction between Convective Instabilities from the Horizontal Section and Taylor Görtler Vortices in Inclined Section

The steam was injected into a pipe of length 5 m with an inclination of 30° degrees from the horizontal axis. The inlet pressure was raised from 10 to 20 bars, whereas the rpm varied from 4,000 till 14,000. The orientation of the pitot tube and the static tube sensors is such that, in each pair of these two sensors, the direction of the pitot tube is parallel to the axial axis of the horizontal section, whereas the static pressure sensor has its front measuring face placed at 90 degrees with the axial axis of the horizontal section as shown in Fig. 9. The elbow channel was just made in order to get a sort of facilitation for the wire/pipe connection with the pitot tube sensor; it's not used to install the sensor in this elbow configuration. The sensor itself is in straight body form for the measurements. In this configuration, we took special care that the flow profiles of the adjacent sensor's pair should not be affected with each other; thus each pair of sensors was installed at a safe distance from each other. As described in previous section, pressure variations were recorded by the static pressure sensors mounted at the wall through the pipe's surface. These variations present wavy like structures, which depict the birth of convective flow instabili-

ties near the wall of the pipe. When the swirly flow of the steam has entered into the inclined pipe section, the vortices in the inclined section can be conveniently referred to as longitudinal curvature induced vortices, also known as Taylor Görtler vortices, which behave differently from convective flow instabilities and this can be seen in Fig. 9. The inception of the Taylor Görtler vortices has been presumed here as these vortices emerged when an imbalance exists between the centrifugal force and radial pressure. Over the concave surface with certain curvature with a fluid flowing with certain velocity, these vortices cast a wave-like behavior at the boundary walls [52].

Pressure profiles were measured at 3 m further from the beginning of the inclined section (at Y=0). The profile, at the bottom of the three profiles in Fig, 9 is attributed to the condition when an inlet pressure of 5 bar for steam and 2,000 rpm has been applied. The purpose of applying lower operating conditions is to examine the effects imparted on the pressure profiles by the two varying operating conditions more clearly and to check the effect of inclination on these two pressure profiles. It has been observed that the convective flow instabilities interact with the Taylor Görtler vortices or inclination induced vortices in a non-linear fashion. As can be seen in Fig. 9, the convective flow instabilities show a decreasing trend for pressure profiles till Y=0; after this a sudden jump has been observed. The nonlinear relation between the two vortices can be explained in the preceding paragraph.

When the pressure was applied at constant rpm, 4,000, starting from ~3 m before the start of the inclined section (Y=0), normalized pressure measurements varied along the boundary wall regions in a wavy like fashion. However, a decreasing trend in pressure measurements can be observed largely, which may be attributed to the overall expansion of the steam as well as steam's pressure drop along the horizontal section. Right from the start of the inclined section, the pressure shows an increasing trend starting with a sudden jump and then increases gradually onwards. This trend was attributed to the contribution by the inclination of the flow channel, which may be represented mathematically by $(\overline{U}+\frac{\partial U}{\partial y})$, using Eq. (1), where the term $\overline{U}$ is the variation in the axial velocity and $\frac{\partial U}{\partial y}$ is the slope of the velocity in the boundary layer flow region. The rise in pressure was observed almost twice of the value of the pressure measured at the point Y=0 for ΔRPM, whereas in the case of the ΔP, this rise in the value was about 70-73%. The wavelength of these vortices in the inclined section was affected as well, as an increase in wavelength of around 16-20% was observed along the axial direction. The flow remained positively skewed throughout the inclined section, which depicts the dominant effect of the longitudinal curvature on the flow skewness. The flow remains positively skewed even when rpm was varied from 4,000 to 14,000.

2-3. Variation in Skin Friction Along the Inclined Channel

To comprehend the impact of the swirling flow past through the channel that has been inclined at an angle of 30° degrees, the skin friction coefficient C_f is an important property of the flow that corresponds constantly to the shape and structure of the flow. Here our emphasis is on the region traversed by a fluid volume ranging from $\sim\frac{2r}{3}$ till r. The shear stress in the boundary wall region was calculated from the slope of the mean velocity within the boundary wall regions. In the horizontal section, the axial velocity was estimated from Eq. (1) [33], whereas in the inclined section it was calculated by Eq. (11) [53],

$$\frac{V_{stagnation}}{V_{static}}=\left[\frac{(P_{stag}-P_{ref})}{(P_{ref}-P_{stat})}+e^{-2ky}\right]^{\frac{1}{2}} \tag{11}$$

Here in Eq. (11), $k=\frac{1}{\text{Radius of curvature}}$. τ_w is wall shear stress and is related to the frictional pressure drop ΔP_f by [54],

$$\frac{\tau_w d^2}{4\rho v^2}=f\left(\frac{\Delta P_f d^2}{4\rho v^2}\right) \tag{12}$$

whereas,

$$\Delta P=P_2-P_1 \tag{13}$$

where P_2 & P_1 are the two consecutive pressure sensors. τ_w is wall shear stress, d is the outer diameter of the pitot tube pressure sensor, ρ is the density of the steam which is considered here as constant, v is the steam's kinematic viscosity. The wall shear stress values which were estimated from the reference, stagnation and static pressure measurements near and at the wall of the horizontal and inclined curved channel using the pitot tube pressure sensor, were used to calculate the skin friction coefficient [54],

$$C_f=\frac{\tau_w}{0.5\rho U_m^2} \tag{14}$$

where, C_f is the local skin friction coefficient, and U_m is the bulk axial velocity. The profiles thus plotted for the local skin coefficient are shown in Fig. 10.

The profiles for the local skin friction have shown a decreasing trend along with the 3 m patch of length approximately till point at Y=0; afterward, the local skin friction shows an increasing trend till the end of the inclined pipe. The profile for the skin friction under the effect of the variation in rotational speed, stretches over more length scale as compared to the case when the inlet pressure was varied from 10 to 20 bars, yet at every spatial position, the value of the skin friction for the ΔRPM is greater than its value under the effect of ΔP. This may be due to the negatively skewed flow, which expels more fluid volume towards the boundary walls. So more chaotic activity was observed in the near boundary wall layers' flow for ΔRPM as compared to ΔP, yet skin friction decreases along the horizontal section till its end at Y=0, but on average the value of C_f for the ΔRPM as compared to ΔP remains higher. Afterward, due to an inclined flow path, skin friction shows an exponential increase for both cases showing region of most chaotic activity for ΔP and ΔRPM. Both profiles have smooth shape yet keep their slopes positive to some extent in the end section of the inclined pipe. A possible reason for this may be the boundary layers being developed at the end of the inclined pipe, whereas the values of the skin friction under the effect of ΔP are higher than the values for the skin friction under the effect of ΔRPM. This is due to divergence of the flow in case of ΔP, causing the flow drift-

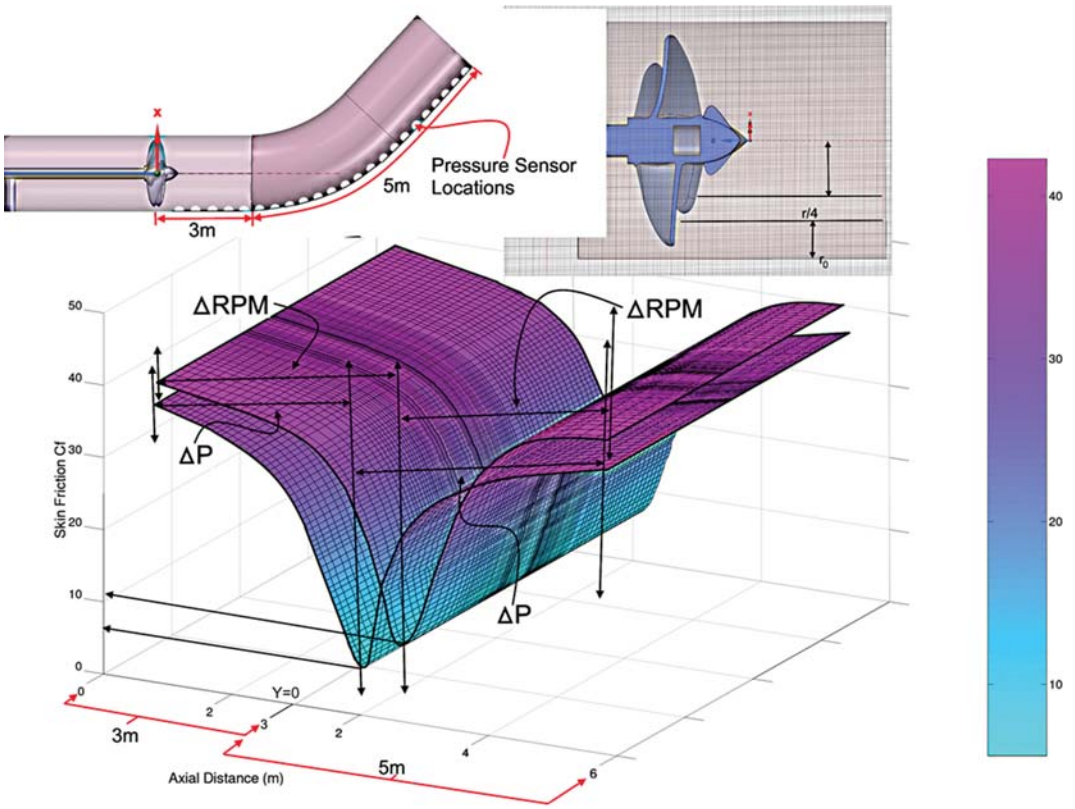

Fig. 10. Local skin friction C_f at varied inlet steam pressure and rotational speed (rpm).

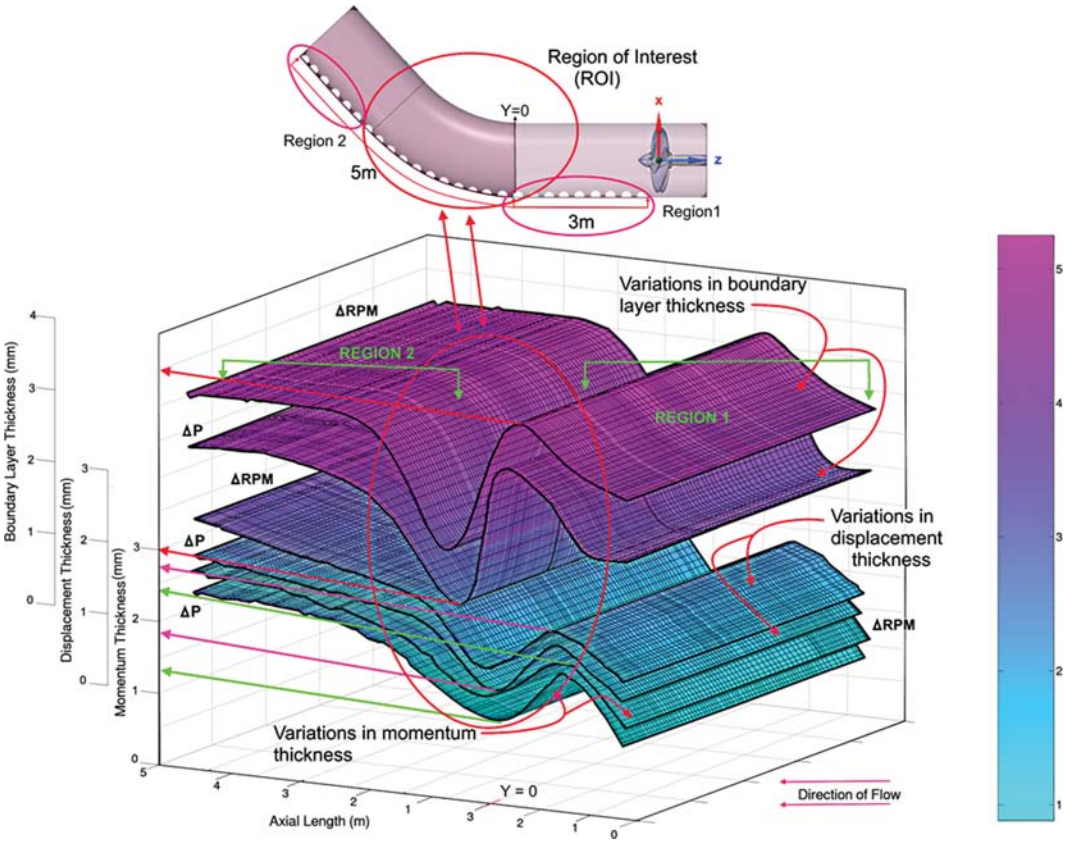

Fig. 11. Profiles for the variations in boundary layer thickness, displacement thickness and momentum layer thickness.

ing more towards inside into the annular region near to central axis [14]. Along the end section of the inclined pipe, the higher values of the skin friction for ΔP may also be due to the flow here has squeezed the fluid further.

2-4. Variations in Turbulence Dissipation Layer Thickness Within the Wall Regions

Variations in the turbulence dissipation layer across boundary wall regions can be measured by estimating the variations in the boundary layer thickness, displacement thickness, and momentum thickness. In the horizontal section, we already have discussed the effect of the variations in inlet steam pressure and rotational speed on these quantities; here in the inclined section, profiles, representing the variations in these quantities under the effect of variations in the input parameters, can be seen in Fig. 11.

It has been observed that all the three profiles for the boundary layer thickness, displacement thickness and momentum thickness under the effect of inlet steam pressure and rotational speed of the propeller show almost similar trends. Boundary layer thickness shows a gradual increase in the boundary layer in region 1. Since, moving far from the propeller at fixed rpm and varying pressure, the favorable pressure drop in the region 1 results into a gradual rise of the boundary layer in this region. After region 1, when the fluid enters the inclined section, the boundary layer thickness drops considerably, which is due to the adverse pressure gradient which is revived back in the region 2 towards the end of inclined section. The displacement thickness and momentum thickness show almost same behavior as the boundary layer thickness; however, the boundary layer thickness fluctuates between ~2.3→5.7 mm, whereas the values of the displacement thickness lie in the range ~1.5→2.5 mm, and values of the momentum thickness layer fluctuate between ~1→2.3 mm. Thus, it can be inferred here that the turbulence dissipation layer within in the region 1 expanded a little before it entered ROI, where it narrowed appreciably and finally in the region 2, the turbulence dissipation layer slowly and gradually recovered. All these profiles have exhibited non-frozen behavior, i.e.,the ROI moves forward (in case for ΔRPM, towards left-hand side in Fig. 11) and backward (in case for ΔP, towards the right-hand side in Fig. 11). It was also observed in repeated experiments that the spatial location of these regions 1 and 2 is not fixed. The non-frozen behavior of all profiles can be attributed to the asymmetric propagation of the steam driven Taylor Görtler vortices in axial direction.

2-5. Dissipated Energy Content of the Turbulent Fluctuations along with the Wall of the Horizontal and Inclined Section

Turbulence inside the flowing fluids is composed of different types of motions, including rotational or compressive, that interact with each other at different scales. When a fluid is driven by means of a propeller with either positive or negative skewness, the instabilities thus formed within the fluid dissipate at different length scales. These instabilities interact with each other in a non-uniform fashion (i.e., convective flow instabilities coupling/interaction with the Taylor Görtler instabilities inside horizontal and then inclined flow channel). Yet at higher speed of the propeller or higher inlet steam pressure or inclination that may contribute to the turbulence in one way or the other, there is negligible effect on the dissipation of these instabilities due to the physical properties of the

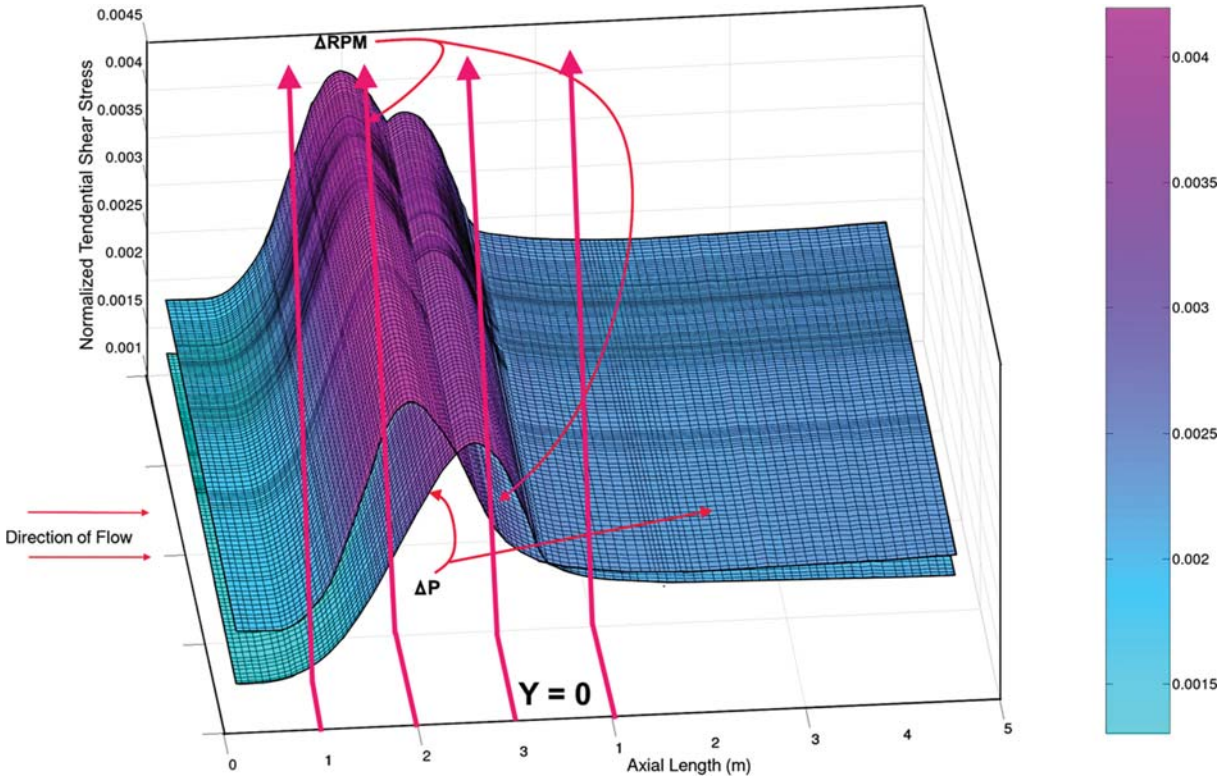

Fig. 12. Profiles for the variations in normalized tangential shear stress along axial direction in horizontal and inclined flow channel.

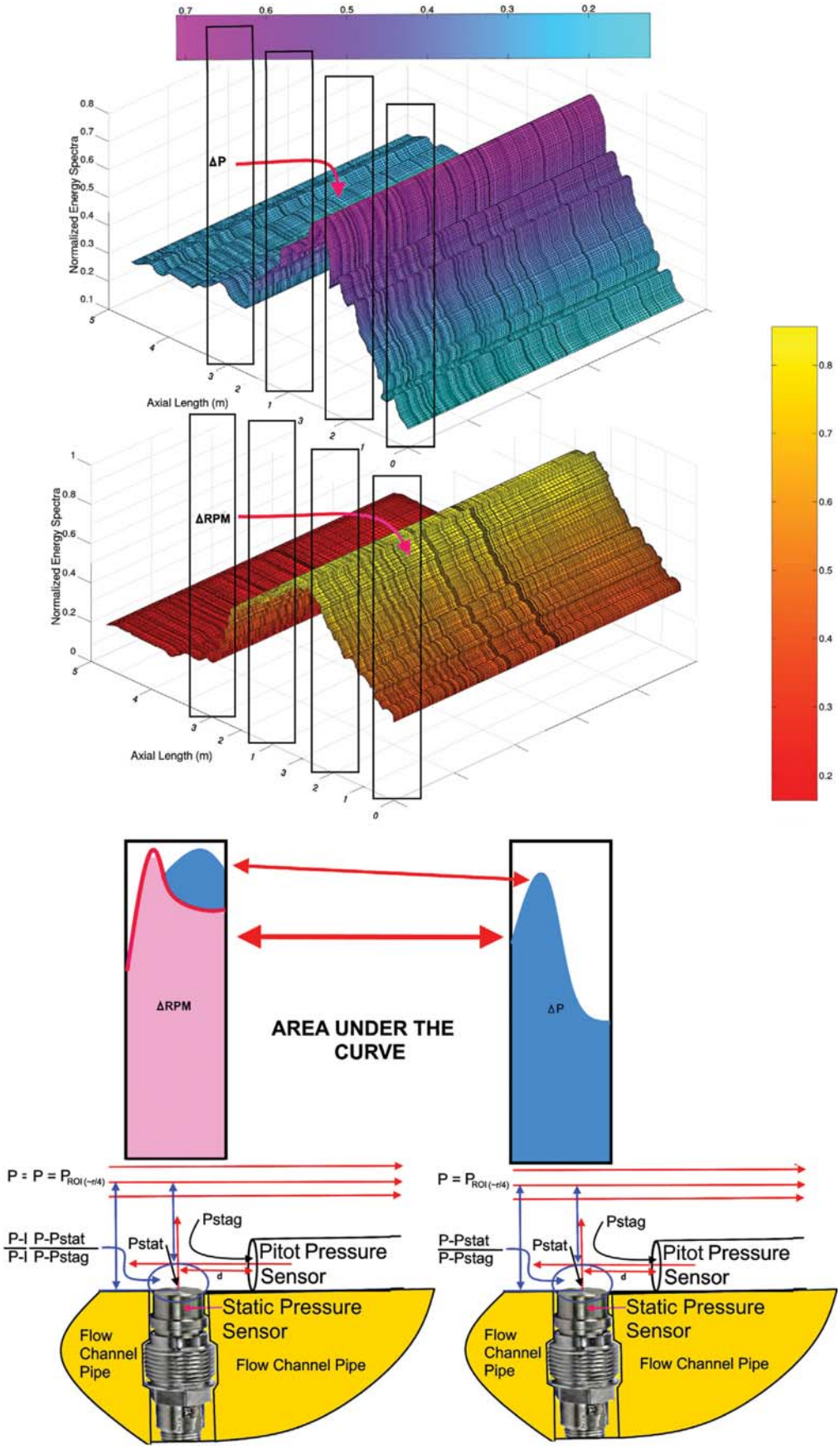

Fig. 13. Normalized energy spectra profiles for variations in inlet steam pressure and rotational speed.

fluids, rather at smaller Kolmogorov scale (comparable to molecular scale), these instabilities dissipate into the fluid regions very near to the wall, thus imparting their heat or vibrating effects.

Variations in the values of the velocities all along the axial positions were calculated from the pressure measurements by the pitot tube and static pressure sensors, along with using Eqs. (1) and (11). The amplitudes of these fluctuations were added in a sequence to draw the profiles shown in Fig. 12. Using the best fit line curves to the lowest values of following two sequences drawn under the effect of inlet pressure of steam and rotational speed of the propeller. Here a series of four points shown by the arrows in vertically upward direction were used to show the multiple positions at left and right of the point Y=0, as shown in Fig. 12. These pressure fluctuations being depicted by the convective flow instabilities and then by the Taylor Görtler vortices in the previous section have a non-frozen behavior on spatial and temporal basis, A dissipation (Kolmogorov) wavenumber [55,56] can be expressed as,

$$K_d = \langle \rho \rangle^{1/2} (\mathrm{Re}^3 \varepsilon) \tag{15}$$

$$\text{where, } \varepsilon = \frac{1}{\mathrm{Re}} \left(\frac{4}{3} \langle \Delta^2 \rangle + \langle |\omega|^2 \rangle \right) \tag{16}$$

where ω has been taken as the angular velocity of the propeller here, expressed as,

$$\Delta = \nabla \cdot U_m \tag{17}$$

And the characteristic energy spectrum is given by,

$$E_0 = \frac{1}{\langle \rho \rangle^{1/2}} \left(\frac{\varepsilon}{\mathrm{Re}^5} \right)^{1/4} \tag{18}$$

where the density is considered constant here, the normalized energy was obtained by dividing the energy values with the kinetic energy of the steam at the inlet of the flow channel, i.e., $\left(\frac{E_0}{\frac{1}{2} m_{steam\ at\ inlet} U_m^2} \right)$ to draw the whole spectrum of energy dissipated axially. The normalized energy was plotted against the normalized waves number as shown in Fig. 13. The area under each curve shows the energy content being dissipated within the region. The profiles are marked with four rectangular bars which show the area under the profile associated with the dissipated energy on those specified locations. Yet the whole of the axial length starting from position at x=7 m from the top left side of this flow channel till the end of the inclined channel is characterized by the pressure sensors installed at equal distance from each other (as explained in detail in experimental section). Here, the purpose of the rectangular bars is to show an array of area under the profiles, giving overlapping spike profiles as shown at the bottom of Fig. 13. The profiles corresponding to ΔP and ΔRPM show a type of continuous surface rather than vertically parabolic profiles for respective sensors. As the pressure sensors are nearly placed, so that the data in terms of variation in normalized energy spectra against the spatial length has an overlapping nature. This can be seen at the bottom of Fig. 13, where the region across the rectangular bars shows the area covered under the respective section of profiles having an overlapping nature, so only those readings that cover the top of the profiles have been considered for plotting these profiles.

These profiles also show amplification of the turbulence dissipation in the region around Y=0. From the profiles for ΔP and ΔRPM, it has been observed that the compressible dissipation rate of energy varies along the radial direction with the force ratio $\frac{F_R}{F_C}$, (of the rotational to the compression components) that corresponds to the excitation of the fluid layers in the region ranging from r=0→r=r. Until this stage, we are not sure how much this dissipation rate be dependent on the vortices induced motion or any other mechanism for excitation. The normalized dissipation energy spectra corresponding to rpm show an increasing trend from position 0 m till ~3.5 m on the axial length scale in the horizontal section as well as a small portion of the inclined section, whereas afterward, till the end of the inclined section it shows a decreasing trend. Also observed is that with an increase in normalized wave number, which was attributed due to variation in rpm, further rise in the dissipation of normalized energy spectra was observed, i.e., in the case of ΔRPM, this change amounts to ~0.9 as compared to the case of ΔP, where only ~0.74 on normalized dissipation energy scale. The exact effective contribution by the centrifugal/rotational forces, as compared to the compressive forces in terms of giving rise to the dissipation of the energy, is not confirmed. However, this is the first time that the role of these forces (when both acting, i.e., at 10-20 bars @ 4,000 rpm & 4,000-14,000 rpm @ 10 bars) have been estimated quantitatively in case of swirling steam flowing across a pipe with horizontal and inclined length sections.

CONCLUSION

Steam was flowed through a pipe with horizontal and inclined sections, at a varying inlet pressure of 10-20 bars using a propeller revolving at rotational speed ranges from 4,000 rpm till 14,000 rpm. While characterizing the flow in horizontal and inclined sections of the flow pipe, convective flow instabilities were observed which have been highlighted in terms of variations in wavelength and profiles across spatial length scale. These flow instabilities propagated through the horizontal and inclined sections in a non-linear fashion. An optimization point was found among the operating conditions based on the intersection of the shear stress profiles. Flow transformed from positive to negative skewness, when the rotational speed of the propeller was raised from 4-14 thousand per minute. More area came under the effect of decreasing skin friction when the rotational speed of the propeller was increased. The turbulent energy dissipation profiles collectively showed variations under the effect of the operating conditions, but specifically, the effect of any one of these operating parameters was not found and this facet of R&D on compressible swirling flows near the boundary wall regions still needs further investigation.

ACKNOWLEDGEMENT

The authors are thankful to University Kebangsaan Malaysia (UKM) for their support for this work through Grant [Grant Reference No: MI-2018-008].

REFERENCES

1. E. B. Wallace, US5407305A: Continuous dense phase conveying method utilizing high pressure gas at predetermined gas pressures within a conveying pipe (1993).
2. E. B. Wallace, Continuous dense phase conveying method utilizing high pressure gas at predetermined gas pressures within a conveying pipe (1993).
3. C. G. Caro, N. V. Watkins, P. L. Birch and M. Yacoub, WO2004083706A1 - Tubing and piping for multiphase flow - Google Patents, 2004.
4. F. Kato, T. Onoda and T. Takano, Japanese Patent, JPH (1998).
5. R. N. Meroney, Measurements of Turbulent Boundary Layer Growth over a Longitudinally Curved Surface (1974).
6. T. Tandiono, S. H. Winoto and D. A. Shah, *Phys. Fluids*, **20**, 094103 (2008).
7. T. Tandiono, S. H. Winoto and D. A. Shah, *Phys. Fluids*, **21**, 084106 (2009).
8. T. Tandiono, S. H. Winoto and D. A. Shah, *J. Vis.*, **12**, 195 (2009).
9. H. Mitsudharmadi, S. H. Winoto and D. A. Shah, *Phys. Fluids*, **17**, 124102 (2005).
10. T. Tandiono, S. H. Winoto and D. A. Shah, *Phys. Fluids*, **25**, 104104 (2013).
11. R. Mukund, P. R. Viswanath, R. Narasimha, A. Prabhu and J. D. Crouch, *J. Fluid Mech.*, **566**, 97 (2006).
12. N. R. Tichenor, R. A. Humble and R. D. W. Bowersox, *J. Fluid Mech.*, **722**, 187 (2013).
13. J. D. Swearingen and R. F. Blackwelder, *J. Fluid Mech.*, **182**, 255 (1987).
14. P. Bradshaw, Effects of streamline curvature on turbulent flow, No. AGARD-AG-169. Advisory Group for Aerospace Research and Development Paris (France) (1973).
15. P. Bradshaw, *J. Fluid Mech.*, **63**, 449 (1974).
16. L. Yang, H. Zare-Behtash, E. Erdem and K. Kontis, *Exp. Therm. Fluid Sci.*, **40**, 50 (2012).
17. M. Jayaram, M. W. Taylor and A. J. Smits, *J. Fluid Mech.*, **175**, 343 (1987).
18. W. Flaherty and J. M. Austin, *Phys. Fluids*, **25**, 106106 (2013).
19. J. F. Donovan, E. F. Spina and A. J. Smits, *J. Fluid Mech.*, **259**, 1 (1994).
20. D. R. Smith and A. J. Smits, *Exp. Fluids*, **18**, 363 (1995).
21. K. J. Franko and S. Lele, *Phys. Fluids*, **26**, 024106 (2014).
22. J.-H. Lee and H. J. Sung, *Int. J. Heat Fluid Flow*, **29**, 568 (2008).
23. Z. Harun, J. P. Monty, R. Mathis and I. Marusic, *J. Fluid Mech.*, **715**, 477 (2013).
24. S. Shu and N. Yang, *Chinese J. Chem. Eng.*, **26**, 31 (2018).
25. S. Shu and N. Yang, *Chem. Eng. Sci.*, **181**, 132 (2018).
26. A. Pradhan and S. Yadav, *Procedia Eng.*, **127**, 177 (2015).
27. H. Sajjadi, M. Salmanzadeh, G. Ahmadi and S. Jafari, *Comput. Fluids*, **150**, 66 (2017).
28. H. Sajjadi, M. Salmanzadeh, G. Ahmadi and S. Jafari, *Particuology*, **30**, 62 (2017).
29. A. Fakhari and T. Lee, *Comput. Fluids*, **107**, 205 (2015).
30. LM35 LM35 Precision Centigrade Temperature Sensors, 1999. www.ti.com.
31. M. S. CORPORATION, Pressure Sensor: PCB Model 113B27, PCB Piezotronics (2019).
32. Subsea Technology and Equipments - Oil&Gas Portal, www.Oil-Gasportal.Com. (n.d.).
33. M. K. King, R. R. Rothfus and R. I. Kermode, *AIChE J.*, **15**, 837 (1969).
34. T. E. Stanton, D. Marshall and C. N. Bryant, *Proc. R. Soc. A Math. Phys. Eng. Sci.*, **97**, 413 (1920).
35. J. Džunić, M. S. Petković and L. D. Petković, *Appl. Math. Comput.*, **217**, 7612 (2011).
36. M. S. Petković, B. Neta, L. D. Petković and J. Džunić, *Appl. Math. Comput.*, **226**, 635 (2014).
37. J. R. Sharma and H. Arora, *Appl. Math. Comput.*, **273**, 924 (2016).
38. P. K. Swanee and A. K. Jain, *J. Hydraul. Div.*, **102**(5), 657 (1976).
39. T. G. Lester, *ASHRAE J.*, **44**, 41 (2002).
40. X. Zhang, X. Sun and X. Xin, Vortex Characteristics of Spiral Flow in Pipe, in: Adv. Water Resour. Hydraul. Eng., Springer Berlin Heidelberg, Berlin, Heidelberg, 2163 (2009).
41. D. W. Baker, Decay of swirling turbulent flow of incompressible fluids in long pipes, in: *Proceeding Symp. Flow-Its Meas. Control Sci. Ind.*, 301 (1974).
42. Y. Senoo and T. Nagata, *Bull. JSME*, **15**, 1514 (1972).
43. T. Benson, Dynamic Pressure of a Moving Fluid Element, pp. 1, NASA (2014).
44. C. H. Gibson, G. R. Stegen and R. B. Williams, *J. Fluid Mech.*, **41**, 153 (1970).
45. J. C. Wyngaard, *J. Fluid Mech.*, **48**, 763 (1971).
46. R. A. Antonia and C. W. Van Atta, *J. Fluid Mech.*, **67**, 273 (1975).
47. P. G. Mestayer, C. H. Gibson, M. F. Coantic and A. S. Patel, *Phys. Fluids*, **19**, 1279 (1976).
48. K. R. Sreenivasan and R. A. Antonia, *Phys. Fluids*, **20**, 1986 (1977).
49. R. M. C. So and G. L. Mellor, An experimental investigation of turbulent boundary layers along curved surfaces, NASA (1972).
50. B. R. Ramaprian and B. G. Shivaprasad, *J. Fluid Mech.*, **85**, 273 (1978).
51. A. J. Smits, J. A. Eaton and P. Bradshaw, *J. Fluid Mech.*, **94**, 243 (1979).
52. S. H. Winoto, H. Mitsudharmadi and D. A. Shah, *J. Vis.*, **8**, 315 (2005).
53. R. N. Meroney and P. Bradshaw, *AIAA J.*, **13**, 1448 (1975).
54. G. Zarbi and A. J. Reynolds, *Fluid Dyn. Res.*, **7**, 151 (1991).
55. A. Kolmogorov, The Local Structure of Turbulence in Incompressible Viscous Fluid for Very Large Reynolds Numbers, Izd-vo Akademii nauk SSSR (1941).
56. S. Kida and S. A. Orszag, *J. Sci. Comput.*, **5**, 85 (1990).